Collaborative Similarity Fusion and Consistency Recovery for Incomplete Multi-view Clustering

Bingbing Jiang[1], Chenglong Zhang[1*], Xinyan Liang[2*], Peng Zhou[3], Jie Yang[4], Xingyu Wu[5], Junyi Guan[1], Weiping Ding[6], Weiguo Sheng[1]

[1]Hangzhou Normal University, Hangzhou, China
[2]Shanxi University, Taiyuan, China
[3]Anhui University, Hefei, China
[4]University of Technology Sydney, NSW, Australia
[5]Hong Kong Polytechnic University, Hong Kong SAR, China
[6]Nantong University, Nantong, China
jiangbb@hznu.edu.cn, clzhang123@163.com, liangxinyan48@163.com, zhoupeng@ahu.edu.cn, jie.yang-1@uts.edu.au, xingy.wu@polyu.edu.hk, jonnyguan73@163.com, dwp9988@163.com, w.sheng@ieee.org.

Abstract

As partial samples are often absent in certain views, incomplete multi-view clustering has become a challenging task. To tackle data with missing views, current methods either utilize the data similarity relations to recover missing samples or primarily consider the available information of existing samples, typically facing some inherent limitations. Firstly, traditional solutions cannot fully explore the potential information contained in missing samples due to their omission strategy, leading to sub-optimal graphs. Moreover, most methods mainly focus on data recovery from the view level, ignoring the differences among available/missing samples in various views. To this end, we propose a collaborative Similarity Fusion and Consistency Recovery (SFCR) method, which resolves the incomplete multi-view clustering problem by learning a unified similarity graph and recovering missing samples with consistent structures. Specifically, to learn a reliable graph compatible across views, a novel view-to-sample fusion model is designed to adaptively coalesce the view-wise similarities among available samples, not only preserving the complementarity and consistency among views but also properly balancing different samples. Furthermore, the missing samples are effectively recovered under the guidance of the fused similarity graph, so as to maintain the consistent structure of recovered data across views. In this way, the similarity learning and the missing data recovery benefit from each other in a collaborative reinforcement manner. Meanwhile, SFCR can directly obtain the final clustering labels without additional post-processing. Extensive experiments demonstrate the effectiveness and superiority of SFCR.

Introduction

With the advance of information technology, data generated from multiple sources becomes more accessible in various applications, referred to as multi-view data (Jiang et al. 2023; Fu et al. 2024; Liang et al. 2024; Cao and Xie 2024). By assuming that the information of all views is complete, previous multi-view clustering methods fully use the complementary and consistent information across views and achieve promising performance (Xue et al. 2019; Li et al. 2022; Gan et al. 2022; Wang et al. 2024a). However, in practical scenarios, multi-view data often encounter incompleteness (i.e., partial samples are absent in some views) due to the instability of external environments and collection processes, affecting the consistent structure among views and causing information loss (Xue et al. 2021). Therefore, incomplete multi-view clustering has become a fundamental yet challenging task (Jiang, Luo, and Liang 2024).

To apply traditional solutions to incomplete multi-view data, the direct way is to fill missing data with the means of available samples or the zeroes. However, this manner fails to consider the potential similarity relations between available samples and missing samples, and the recovered samples might be noises, impairing the truth relations among samples. Therefore, several researchers have made efforts to deal with incomplete multi-view data. For example, (Trivedi et al. 2010) presented a kernel canonical correlation analysis method to recover the kernel matrix with missing views; (Li, Jiang, and Zhou 2014) exploited the non-negative matrix factorization to learn a latent representation that divides samples into complete parts and view-specific missing parts. However, these methods are specially designed for two-view incomplete data, constraining their applicability as the number of views increases (Wen et al. 2019).

To directly tackle the incomplete data with multiple views, many methods have been developed, which can be grouped into two ways according to how to handle missing samples. The first way directly discards missing samples and concentrates on exploring the view-specific information among available samples. Representative methods include adaptive weighted graph fusion (Zhang et al. 2020) and projective incomplete multi-view clustering (Deng et al. 2024), which typically involve the following steps: learning latent representations for available samples on each view, aligning them based on the known missing index, and integrating the view-specific representations to learn a unified one. Al-

*The corresponding authors.

though achieving some progress, they instinctively abandon missing samples, impairing the learning of consensus relations and compromising ultimate clustering.

To alleviate this issue, another way attempts to leverage the intrinsic relations among samples or views to recover missing data (Zhang et al. 2023b) and learns a unified representation from multiple views. Specifically, (Wen et al. 2019) proposed the unified embedding alignment with missing views inferring, which recovers the samples with missing views by the correlations among views. (Liu et al. 2021) employed the similarity relations of samples to guide the recovery, such that the missing samples can be predicted by their nearby available samples. (Yin and Sun 2023) utilized the common latent representation to impute the missing samples in each view separately. Inheriting from (Liu et al. 2021), (Wang et al. 2024b) proposed to leverage the global and view-specific similarity structures to facilitate the missing samples learning. Nevertheless, these recovery-based methods either treat different views equally or simply discriminate them at the view level. Considering that incomplete multi-view data involves the aspects of samples and views, thus the current recovery model mainly focuses on missing views yet overlooks the differences among available/missing samples across views, affecting the ultimate clustering processes. Moreover, most methods recover missing samples within each view independently, overlooking the consistent similarity structure across views. Besides, existing methods require post-processing (e.g., K-means) on learned representation or recovered data to obtain the final results, not only increasing computational burden but also making their performance subject to K-means clustering.

Based on the above analyses, two factors limit the performance of existing incomplete multi-view clustering methods. On the one hand, the recovery-based methods neglect the differences of samples from diverse views. On the other hand, the consistency of inherent structures on recovered samples in different views is not considered in the procedures of data recovery. Motivated by these limitations, we propose a collaborative Similarity Fusion and Consistency Recovery (SFCR) for incomplete multi-view clustering. Figure. 1 illustrates the basic framework of SFCR, and the main contributions of this paper are summarized as follows:

- We propose a novel incomplete multi-view clustering method, which jointly incorporates the view-to-sample similarity fusion, missing data recovery with consistency structure, and multi-view clustering into a unified framework, improving the ultimate clustering performance.
- An adaptive fusion model is devised, which not only introduces the view-to-sample weight to discriminate available/missing samples but also implicitly measures the importance of each view on graph learning, positively enhancing the reliability of similarity graphs.
- The missing data recovery is under the guidance of the learned similarity graph, guaranteeing the consistent structure of recovered samples across multiple views. Moreover, a rank constraint is imposed on the learned graph to directly provide the clustering labels, thereby avoiding the post-processing.

Notation	Description
n_v	The number of v-th view available samples
n	The number of total training samples
d_v	The dimension of v-th view
c	The number of classes
V	The number of views
$\mathbf{X}_o^v \in \mathbb{R}^{d_v \times n_v}$	The available samples in v-th view
$\mathbf{X}_m^v \in \mathbb{R}^{d_v \times n - n_v}$	The missing samples in v-th view
$\mathbf{X}^v \in \mathbb{R}^{d_v \times n}$	The v-th view samples
$\mathbf{\Phi} \in \mathbb{R}^{n \times v}$	The available sample indices matrix
$\mathbf{G}^v \in \mathbb{R}^{n \times n_v}$	The missing index matrix in v-th view
$\mathbf{1} \in \mathbb{R}^{c \times 1}$	The all-one vector

Table 1: Description of Notations

Methodology

In this section, we propose a novel incomplete multi-view clustering with collaborative similarity fusion and consistency recovery, whose crucial details are elaborated.

Notations

Throughout the paper, matrices and vectors are written in uppercase and lowercase bold letters, respectively. In the incomplete environment, partial samples are absent in some views, such that the missing index matrix $\mathbf{G}^v \in \mathbb{R}^{n \times n_v}$ for the v-th view is defined as:

$$g_{ij}^v = \begin{cases} 1, \text{if } j\text{-th available instance } x_j^v \text{ belongs to } i\text{-th sample}, \\ 0, \text{otherwise}. \end{cases}$$

$\mathrm{Tr}(\mathbf{M})$ denotes the trace of $\mathbf{M}$ and $\|\mathbf{M}\|_F = \sqrt{\mathrm{Tr}(\mathbf{M}^T\mathbf{M})}$ represents the Frobenius norm. Table 1 lists the frequently used notations.

View-to-sample Similarity Fusion and Learning

As similarity graphs can effectively preserve the similarity relations among samples (Hu et al. 2022; Zhang et al. 2023a; Jiang et al. 2024), many graph-based clustering methods have been proposed. Noting that traditional methods utilize pre-constructed graphs to guide subsequent tasks, such that the interaction between graph learning and clustering is entirely ignored, which impairs the clustering effectiveness (Wen et al. 2022). To this end, we propose to dynamically learn the graph during the clustering process under the incomplete setting. Specifically, the view-specific similarity relations between available samples in v-th view can be captured as follows:

$$\min_{\widetilde{\mathbf{S}}^v\mathbf{1}=\mathbf{1}, \widetilde{\mathbf{S}}^v \geq 0, \mathrm{diag}(\widetilde{\mathbf{S}}^v)=0} \sum_{i,j=1}^{n_v} \|\mathbf{x}_{oi}^v - \mathbf{x}_{oj}^v\|_2^2 \widetilde{s}_{ij}^v + \tau \|\widetilde{\mathbf{S}}^v\|_F^2, \quad (1)$$

where $\widetilde{\mathbf{S}}^v \in \mathbb{R}^{n_v \times n_v}$ is the similarity graph of available samples on the v-th available. Eq.(1) can be directly solved by an adaptive neighbor strategy (the number of neighbors is set to 15) (Nie, Wang, and Huang 2014), and the incomplete graphs can be transformed into the complete graphs by: $\mathbf{S}^v = \mathbf{G}^v \widetilde{\mathbf{S}}^v \mathbf{G}^{vT} \in \mathbb{R}^{n \times n}$.

To explore similarity structures across views, existing incomplete multi-view clustering methods typically treat different views equally or differentiate views with the view weights, concentrating on the discrepancies at the view

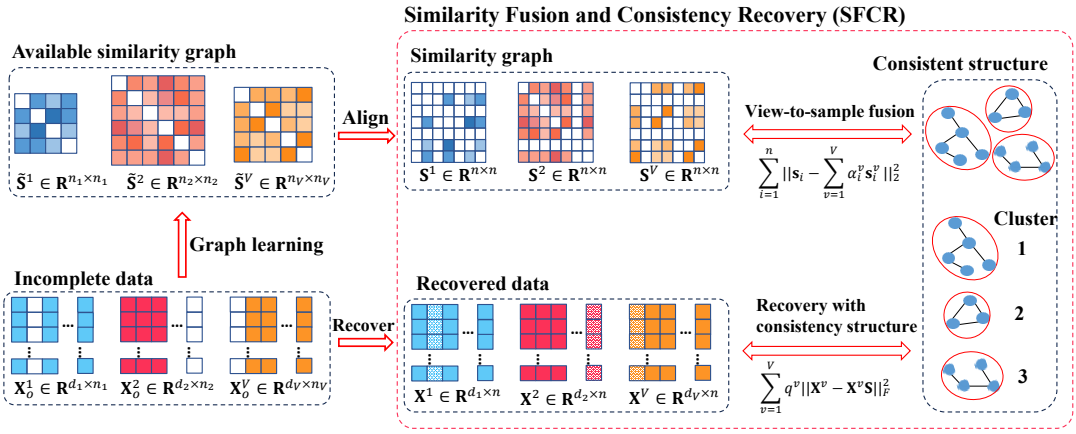

Figure 1: Schematic illustration of SFCR. Firstly, the similarity relations among available samples are captured and aligned to explore the view-specific information. Afterward, the view-to-sample weights are leveraged to fuse similarities while discriminating different samples. Further, the similarity graph and recovery of missing samples are collaboratively enhanced, maintaining a consistent structure across views. Finally, the clustering labels can be directly obtained without post-processing.

level. However, the incomplete multi-view problem involves the aspects of samples and views since partial samples are missing in certain views, the previous method mainly focuses on the information fusion from the view perspective, which is unreasonable especially when the missing ratios increase. Therefore, a view-to-sample similarity fusion model that fully considers the contribution diversity of each sample from different views is devised as follows:

$$\min_{\mathbf{S1}=\mathbf{1},\mathbf{S}\geq 0,(\mathbf{\Phi}\odot\boldsymbol{\alpha})\mathbf{1}=\mathbf{1},\boldsymbol{\alpha}\geq 0}\sum_{i=1}^{n}\|\mathbf{s}_i-\sum_{v=1}^{V}\alpha_i^v\mathbf{s}_i^v\|_2^2, \tag{2}$$

where s_{ij} represents the consistent similarity between the i-th and j-th samples across views. $\mathbf{\Phi}\in\mathbb{R}^{n\times v}$ denotes the available sample index matrix, in which $\Phi_{iv}=1$ if the i-th sample is available in v-th view and $\Phi_{iv}=0$ otherwise. $\boldsymbol{\alpha}_i=[\alpha_i^1,...,\alpha_i^v]\in\mathbb{R}^{1\times v}$ measures the importance of the i-th sample in different views. Unlike existing methods that overlook the differences between samples across multiple views, Eq. (2) introduces view-to-sample weights to assess the importance of available/missing samples in each view, exploring the consistent information from available samples.

Recovery with Consistency Structure

To achieve incomplete multi-view clustering, traditional solutions propose to utilize zeros or sample means to fill the absent samples, which has been proven to distort the intrinsic structure of data (Wen et al. 2019). Considering that the high similarity relations indicate that samples have closer structure distributions (i.e., attributions), a consistent self-representation recovery model is proposed as follows:

$$\min_{\mathbf{X}_o^v=\mathbf{X}^v\mathbf{G}^v,\mathbf{S1}=\mathbf{1},\mathbf{S}\geq 0,\mathrm{diag}(\mathbf{S})=0}\sum_{v=1}^{V}\|\mathbf{X}^v-\mathbf{X}^v\mathbf{S}\|_F. \tag{3}$$

In Eq. (3), $\mathbf{X}^v$ is treated as a variable, where the available samples are set to the true attributions (i.e., $\mathbf{X}_o^v=\mathbf{X}^v\mathbf{G}^v$), and the missing samples are imputed through self-representation under the guidance of consistent similarity structure, such that the locality within samples can be effectively preserved. Meanwhile, Eq. (3) implicitly distinguishes multiple views to learn a unified graph $\mathbf{S}$ by virtue of the matching degrees between $\mathbf{X}^v$ and $\mathbf{X}^v\mathbf{S}$, which effectively enhances the robustness of $\mathbf{S}$. The Lagrangian function of Eq. (3) is:

$$\sum_{v=1}^{V}\|\mathbf{X}^v-\mathbf{X}^v\mathbf{S}\|_F+\mathbf{L}(\mathbf{\Lambda},\mathbf{S}), \tag{4}$$

where $\mathbf{\Lambda}$ denotes the Lagrange multipliers, and $\mathbf{L}(\mathbf{\Lambda},\mathbf{S})$ is a formalized term derived from the constraints. Taking the derivative of Eq. (4) w.r.t. $\mathbf{S}$ and setting it to zero, we have

$$\begin{aligned}&\sum_{v=1}^{V}\frac{\partial\|\mathbf{X}^v-\mathbf{X}^v\mathbf{S}\|_F}{\partial\mathbf{S}}+\frac{\partial\mathbf{L}(\mathbf{\Lambda},\mathbf{S})}{\partial\mathbf{S}}=0\\ \Rightarrow&\sum_{v=1}^{V}q^v\frac{\partial\|\mathbf{X}^v-\mathbf{X}^v\mathbf{S}\|_F^2}{\partial\mathbf{S}}+\frac{\partial\mathbf{L}(\mathbf{\Lambda},\mathbf{S})}{\partial\mathbf{S}}=0,\end{aligned} \tag{5}$$

where $q^v=\frac{1}{2\|\mathbf{X}^v-\mathbf{X}^v\mathbf{S}\|_F}$. Therefore, Eq. (3) essentially boils down to the following problem:

$$\min_{\mathbf{X}_o^v=\mathbf{X}^v\mathbf{G}^v,\mathbf{S1}=\mathbf{1},\mathbf{S}\geq 0,\mathrm{diag}(\mathbf{S})}\sum_{v=1}^{V}q^v\|\mathbf{X}^v-\mathbf{X}^v\mathbf{S}\|_F^2, \tag{6}$$

which can be solved by alternately updating $\mathbf{S}$ and q^v, properly balancing the contribution diversity among views.

Overall Model of SFCR

Theorem 1. *The number of the eigenvalue 0 of the graph Laplacian matrix $\mathbf{L}_S$ is equal to the number of connected components in the graph $\mathbf{S}$.* (Mohar et al. 1991)

To separate samples into c clusters, the ideal graph structure should have the same number of connected components (Nie, Wang, and Huang 2014). According to Theorem 1, the rank constraint $\mathrm{rank}(\mathbf{S})=n-c$ is imposed on the learned graph $\mathbf{S}$, which can be achieved by solving the following problem (Fan 1949):

Algorithm 1: Optimization procedures for SFCR

Input: Incomplete multi-view data $\mathbf{X}$, index matrices $\{\mathbf{G}^v\}_{v=1}^V$, clustering number c and parameter λ;

Initialize the view-to-sample weights $\alpha_i^v = 1/V$, learn graphs of available samples $\{\widetilde{\mathbf{S}}^v\}_{v=1}^V$ by Eq. (1) and construct the complete graphs by $\mathbf{S}^v = \mathbf{G}^v\widetilde{\mathbf{S}}^v\mathbf{G}^{vT}$;

repeat

  Update $\mathbf{X}_m^v$ by Eq. (12);

  Update $\mathbf{S}$ by solving Eq. (15);

  Update $\mathbf{F}$ by solving Eq. (16);

  Update $\boldsymbol{\alpha}$ by solving Eq. (19);

  Update β by Eq. (20);

until Eq. (8) converges;

Output: The clustering labels are derived from the graph structure of $\mathbf{S}$, which has c connected components.

$$\min_{\mathbf{X}^v,\mathbf{S},\mathbf{F}} \sum_{v=1}^{V} q^v \|\mathbf{X}^v - \mathbf{X}^v\mathbf{S}\|_F^2 + \beta \mathrm{Tr}(\mathbf{F}^T\mathbf{L}_s\mathbf{F})$$
$$\text{s.t. } \mathbf{X}_o^v = \mathbf{X}^v\mathbf{G}^v, \mathbf{S}\mathbf{1} = \mathbf{1}, \mathbf{S} \geq 0, \mathrm{diag}(\mathbf{S}) = 0, \mathbf{F}^T\mathbf{F} = \mathbf{I}, \quad (7)$$

where $\mathbf{F} \in \mathbb{R}^{n\times c}$ can be regarded as the unified representation of samples. In Eq. (7), β controls the number of connected components, which can be dynamically updated during optimization procedures. By incorporating the view-to-sample similarity fusion, data recovery via consistency structure, and multi-view clustering into a unified framework, the final objective of SFCR is formulated as:

$$\min_{\mathbf{X}^v,\mathbf{F},\mathbf{S}\geq 0,\mathrm{diag}(\mathbf{S})=0,\boldsymbol{\alpha}\geq 0} \sum_{i=1}^{n} \|\mathbf{s}_i - \sum_{v=1}^{V} \alpha_i^v \mathbf{s}_i^v\|_2^2 + \beta \mathrm{Tr}(\mathbf{F}^T\mathbf{L}_s\mathbf{F})$$
$$+\lambda \sum_{v=1}^{V} q^v \|\mathbf{X}^v - \mathbf{X}^v\mathbf{S}\|_F^2$$
$$\text{s.t. } \mathbf{X}_o^v = \mathbf{X}^v\mathbf{G}^v, \mathbf{S}\mathbf{1} = \mathbf{1}, \mathbf{F}^T\mathbf{F} = \mathbf{I}, (\boldsymbol{\Phi} \odot \boldsymbol{\alpha})\mathbf{1} = \mathbf{1}. \quad (8)$$

Benefiting from the rank constraint, the learned graph has a clear structure, in which the clustering results can be achieved without the post-processing. Moreover, the similarity graph learning and the data recovery collaboratively interact with each other, which not only balances the distinctions among views and samples but also keeps the consistent structure of recovered data across views, providing an effective solution to the dilemma of incomplete data.

Optimization and Analysis

To address the non-joint convex problem in Eq. (8), an iterative strategy is designed to optimize one variable while fixing others. The detailed procedures are provided:

• $\mathbf{X}^v$ **subproblem:** Fixing other variables, the subproblem of Eq. (8) w.r.t. $\mathbf{X}^v$ becomes:

$$\min_{\mathbf{X}_o^v = \mathbf{X}^v\mathbf{G}^v} \|\mathbf{X}^v - \mathbf{X}^v\mathbf{S}\|_F^2. \quad (9)$$

For convenience, we can rewrite the $\mathbf{X}^v$ and $\mathbf{S}$ based on the available/missing index as: $\bar{\mathbf{X}}^v = [\mathbf{X}_o^v, \mathbf{X}_m^v]$, $\bar{\mathbf{S}} = \begin{bmatrix} \mathbf{S}_{oo} & \mathbf{S}_{om} \\ \mathbf{S}_{mo} & \mathbf{S}_{mm} \end{bmatrix}$, and Eq. (9) can be transformed into:

$$\min_{\mathbf{X}_m^v} \mathrm{Tr}([\mathbf{X}_o^v, \mathbf{X}_m^v](\mathbf{I} - \bar{\mathbf{S}})(\mathbf{I} - \bar{\mathbf{S}})^T[\mathbf{X}_o^v, \mathbf{X}_m^v]^T). \quad (10)$$

Denoting $(\mathbf{I} - \bar{\mathbf{S}})(\mathbf{I} - \bar{\mathbf{S}})^T$ as $\mathbf{A}$, whose block matrix form is $\mathbf{A} = \begin{bmatrix} \mathbf{A}_{oo} & \mathbf{A}_{om} \\ \mathbf{A}_{mo} & \mathbf{A}_{mm} \end{bmatrix}$. Therefore, Eq. (10) becomes:

$$\min_{\mathbf{X}_m^v} \mathrm{Tr}(\mathbf{X}_m^v\mathbf{A}_{mm}\mathbf{X}_m^{vT} + 2\mathbf{X}_o^v\mathbf{A}_{om}\mathbf{X}_m^{vT}). \quad (11)$$

Taking its derivative w.r.t. $\mathbf{X}_m^v$ to zero, we achieve the optimal solution of $\mathbf{X}_m^v$ as follows:

$$\mathbf{X}_m^v = -\mathbf{X}_o^v\mathbf{A}_{om}\mathbf{A}_{mm}^{-1}. \quad (12)$$

• **S subproblem:** By fixing other variables, the problem of Eq. (8) is simplified into:

$$\min_{\mathbf{S}} \sum_{i=1}^{n} \|\mathbf{s}_i - \sum_{v=1}^{V} \alpha_i^v \mathbf{s}_i^v\|_2^2 + \lambda \sum_{v=1}^{V} q^v \|\mathbf{X}^v - \mathbf{X}^v\mathbf{S}\|_F^2$$
$$+\beta \mathrm{Tr}(\mathbf{F}^T\mathbf{L}_s\mathbf{F}) \text{ s.t. } \mathbf{S}\mathbf{1} = \mathbf{1}, \mathbf{S} \geq 0, \mathrm{diag}(\mathbf{S}) = 0. \quad (13)$$

To solve Eq. (13) efficiently, we set the partial derivative w.r.t $\mathbf{S}$ to zero, obtaining the latent solution $\mathbf{S}^*$ as:

$$\mathbf{S}^* = (\mathbf{I}_n + \mathbf{B})^{-1}(\mathbf{B} + \mathbf{D}), \quad (14)$$

where $\mathbf{B} = \lambda \sum_{v=1}^{V} q^v \mathbf{X}^{vT}\mathbf{X}^v$ and $\mathbf{D} \in \mathbb{R}^{n\times n}$ with $d_{ij} = \sum_{v=1}^{V} \alpha_i^v s_{ij}^v - \frac{\beta}{4}\|\mathbf{f}_i - \mathbf{f}_j\|_2^2$. Then, the optimal solution of $\mathbf{S}$ is achieved by:

$$\min_{\mathbf{S}\geq 0,\mathbf{S}\mathbf{1}=\mathbf{1},\mathrm{diag}(\mathbf{S})=0} \|\mathbf{S} - \mathbf{S}^*\|_F^2, \quad (15)$$

which can be solved by (Nie, Wang, and Huang 2014).

• **F subproblem:** When other variables are fixed, the problem of Eq. (8) is simplified into:

$$\min_{\mathbf{F}^T\mathbf{F}=\mathbf{I}} \mathrm{Tr}(\mathbf{F}^T\mathbf{L}_s\mathbf{F}). \quad (16)$$

Through performing the eigen-decomposition on $\mathbf{L}_s$, $\mathbf{F}$ can be directly obtained by comprising the c eigenvectors corresponding to the c smallest eigenvalues.

• $\boldsymbol{\alpha}$ **subproblem:** When other variables are fixed, the problem of Eq. (8) is simplified into:

$$\min_{(\boldsymbol{\Phi}\odot\boldsymbol{\alpha})\mathbf{1}=\mathbf{1}} \sum_{i=1}^{n} \|\mathbf{s}_i - \sum_{v=1}^{V} \alpha_i^v \mathbf{s}_i^v\|_2^2. \quad (17)$$

Considering that each row of $\boldsymbol{\alpha}$ (i.e., $\boldsymbol{\alpha}_i$) is independent, thus $\boldsymbol{\alpha}$ can be solved by rows:

$$\min_{(\boldsymbol{\Phi}_i\odot\boldsymbol{\alpha}_i)\mathbf{1}=1} \|\mathbf{s}_i - \sum_{v=1}^{V} \alpha_i^v \mathbf{s}_i^v\|_2^2 \Rightarrow \|\sum_{v=1}^{V} \alpha_i^v(\mathbf{s}_i - \mathbf{s}_i^v)\|_2^2. \quad (18)$$

Denoting $\mathbf{c}_i = \mathbf{s}_i - \mathbf{s}_i^v$, Eq. (18) becomes:

$$\min_{(\boldsymbol{\Phi}_i\odot\boldsymbol{\alpha}_i)\mathbf{1}=1,\boldsymbol{\alpha}_i\geq 0} \boldsymbol{\alpha}_i\mathbf{c}_i\mathbf{c}_i^T\boldsymbol{\alpha}_i^T. \quad (19)$$

Eq. (19) is a quadratic programming problem and can be solved efficiently by (Hestenes 1969).

Update β: In each iteration, the parameter β can be dynamically update based on the number of 0 eigenvalues of $\mathbf{L}_s$, which can be formulated as follows:

$$\beta = \begin{cases} 2\beta, & \text{if } \sum_{i=c+1}^{n} \sigma_i > 0 \\ \frac{\beta}{2}, & \text{if } \sum_{i=c+1}^{n} \sigma_i < 0 \end{cases}. \quad (20)$$

where σ_i denotes the i-th eigenvalue. Through Eq. (20), SFCR concentrates on data recovery in the earlier stage and identifies the correct connected components finally. Specifically, the corresponding $\mathbf{S}$ has exact c connected components if $\sum_{i=c+1}^{n} \sigma_i = 0$, and the clustering results can be obtained directly according to the connectedness of $\mathbf{S}$.

Dataset	Classes	Samples	Features
3sources	6	169	10259(3560/3631/3068)
Webkb	4	203	2163(1703/230/230)
MSRC-v1	7	210	2418(1302/48/512/100/256/200)
ORL	40	400	1689(512/59/864/254)
Leaves	100	1600	192(64/64/64)
COIL100	100	7200	90(30/30/30)

Table 2: The detailed information of multi-view datasets.

Computational Complexity Algorithm 1 summarizes the entire steps for addressing the problem in Eq. (8) by iteratively solving each variable. In practice, learning the graph of available samples (i.e., $\widetilde{\mathbf{S}}^v$) by Eq. (1) needs $\sum_{v=1}^{V}\mathcal{O}(n_v^2)$, and transforming them into the complete graphs (i.e., $\mathbf{S}^v$) takes $\sum_{v=1}^{V}\mathcal{O}(n_v)$. Calculating $\mathbf{X}_m^v$ and $\mathbf{S}$ involves the inverse operation, requiring $\mathcal{O}(n_m^{v3}+n_m^{v2}n_o^v+n_m^v n_o^v d)$ and $\mathcal{O}(n^3+n^2 d)$; solving $\mathbf{F}$ involves the eigen-decomposition on the Laplacian matrix $\mathbf{L}_s$, costing $\mathcal{O}(n^2 c)$; Besides, updating $\boldsymbol{\alpha}$ takes $\mathrm{poly}(V)$. Considering that V and c are small constants, the main computational complexity of SFCR is approximated to $\mathcal{O}(n^3+n^2 d)$, which is competitive with state-of-the-art methods.

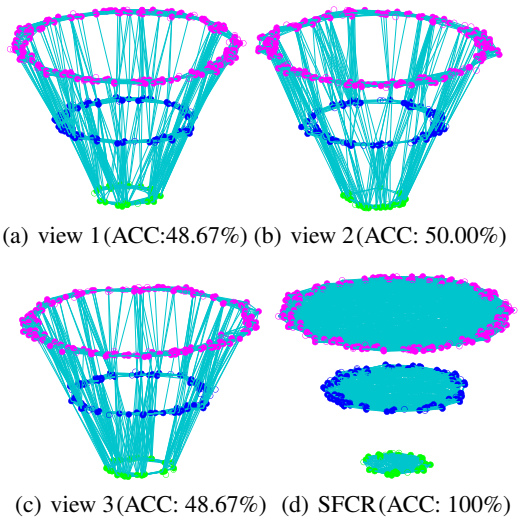

(a) view 1(ACC:48.67%) (b) view 2(ACC: 50.00%)

(c) view 3(ACC: 48.67%) (d) SFCR(ACC: 100%)

Figure 2: Visualization of the Three-Ring. (a)-(c) shows the similarity graphs constructed by Eq. (1) (k=15) of each view, and (d) denotes the learned graph compatible across all views. The accuracies obtained by partitioning each graph into 3 connected components are recorded in parentheses.

Experiments

Experimental Settings

To validate the effectiveness of the proposed SFCR, six real-world datasets are employed, including 3sources (Jiang et al. 2021), Webkb (Wang, Yang, and Liu 2020), MSRC-v1 (Wang, Yang, and Liu 2020), ORL (Zhang et al. 2023b), Leaves (Zhang et al. 2024a) and COIL100 (Zhang et al. 2024b), whose details are summarized in Table 2. Moreover, six state-of-the-art competitors are used to compare with SFCR, including: (1) Best Single View (**BSV**), where the missing samples are presented by $\mathbf{0}$ and the highest results among multiple views are recorded; (2) Unified Embedding Alignment with missing views Inferring (**UEAI**) (Wen et al. 2019); (3) Adaptive Weighted Graph Fusion (**AWGF**) (Zhang et al. 2020); (4) Incomplete Multi-view Self-Representation subspace clustering (**IMSR**) (Liu et al. 2021); (5) Projective Incomplete Multi-View Clustering (**PIMVC**) (Deng et al. 2024); (6) Sample-level Cross-view Similarity Learning (**SCSL**) (Liu et al. 2024). Following the conventions of existing incomplete multi-view clustering works (Liu et al. 2024), the incomplete multi-view data are generated by randomly choosing samples from the complete datasets. Specifically, we vary the incomplete ratio on each view from the range of $\{0\%, 20\%, 30\%\}$, while ensuring every sample appears at least once. For a fair comparison, the parameters of all compared methods are tuned according to the recommended settings in their respective works. In SFCR, β can be dynamically updated based on the number of connection components, thus we initialize $\beta = 1$ and search λ in the grid of $\{10^{-3}, 10^{-2}, \cdots, 10^{3}\}$. Besides, since other methods require the post-precessing to obtain the clustering labels, such that we repeated the K-means 20 times to achieve the average clustering results. All methods have been conducted on different missing groups five times, and the clustering accuracy (ACC) and the normalized mutual information (NMI) are reported to evaluate the performance of different methods. All experiments are conducted in Matlab R2022a on Windows 10 with a 3.2GHz CPU and 32GB RAM.

Experiments on Synthetic Dataset

To demonstrate the effectiveness of the proposed view-to-sample graph learning and fusion model, we conduct experiments on the Three-Ring dataset with three views (Zhan et al. 2018), and each view has three clusters with 30, 90 and 180 samples, respectively. Specifically, Figures. 2 (a)-(c) are the initialized graphs on three views, and Figure. 2 (d) represents the consistent graph learned by SFCR. We find that different clusters exist many connections in the initial graph since the incomplete scenario impairs the real relations between samples. In contrast, benefiting from the collaborative similarity fusion and consistency recovery, the adverse influences of missing samples are effectively reduced, such that the unified graph learned by SFCR can depict the relation between samples more accurately (i.e., different clusters can be explicitly separated without any connecting lines), enhancing the effectiveness of the ultimate clustering.

Experiments on Real-world Datasets

To comprehensively evaluate the performance of incomplete multi-view clustering methods, the means and stds of ACC and NMI on six real datasets are presented in Table 3, and Table 4 shows the average ranks of each method across different missing ratios. Specifically, there are no stds when the missing ratio is fixed at 0%, as the missing group is unique. Considering SCSL requires the feature dimension of each view to be larger than the class number, making it

ACC of each method across varied missing ratios									
Method \Ratio	3sources			Webkb			MSRC-v1		
	0	20	30	0	20	30	0	20	30
BSV	57.16	50.97±1.27	44.52±1.24	71.28	64.55±1.77	62.45±2.69	73.57	61.04±2.52	53.07±1.34
UEAI	63.91	62.81±3.78	61.40±7.64	73.40	72.90±3.84	**71.80**±4.08	91.90	88.87±1.54	85.85±2.16
AWGF	68.05	64.60±4.45	63.91±4.40	71.43	57.73±8.49	55.17±4.44	84.29	80.41±5.70	77.00±5.87
IMSR	67.04	57.91±7.55	57.54±1.89	67.98	69.49±4.99	69.31±6.43	90.57	89.27±3.42	87.15±3.41
PIMVC	73.20	63.86±2.10	63.16±4.35	69.95	62.39±2.46	60.29±5.04	**95.19**	**92.09**±0.38	87.47±1.68
SCSL	59.05	44.90±2.23	44.44±4.76	68.97	56.63±4.25	48.41±6.39	92.38	84.97±2.24	75.78±3.14
SFCR	**77.52**	**74.67**±1.79	**73.33**±2.32	**74.38**	**73.39**±0.77	71.42±0.67	94.76	91.80±1.23	**89.14**±1.69
Method \Ratio	ORL			Leaves			COIL100		
	0	20	30	0	20	30	0	20	30
BSV	73.33	56.19±1.89	49.14±2.25	60.68	47.09±0.21	39.41±0.49	61.57	50.75±0.72	44.19±0.29
UEAI	74.08	70.01±0.11	68.10±0.66	79.05	64.19±0.46	53.44±0.89	60.67	51.83±0.54	46.64±0.39
AWGF	65.75	59.21±1.47	54.09±2.04	77.94	65.41±1.45	65.21±0.96	60.99	58.61±0.74	55.28±0.89
IMSR	74.78	71.96±1.58	69.48±1.10	80.96	63.36±1.24	53.91±0.69	59.42	52.18±0.46	46.89±0.36
PIMVC	75.45	74.47±0.71	74.19±1.23	81.71	66.85±0.82	66.09±1.13	67.07	68.72±0.36	67.59±0.68
SCSL	78.25	73.99±1.85	69.87±1.60	-	-	-	-	-	-
SFCR	**90.25**	**81.80**±3.22	**77.90**±2.00	**91.19**	**79.51**±1.53	**69.05**±1.83	**81.58**	**73.63**±0.93	**70.99**±2.16

NMI of each method across varied missing ratios									
Method \Ratio	3sources			Webkb			MSRC-v1		
	0	20	30	0	20	30	0	20	30
BSV	51.67	36.48±1.73	32.46±0.58	46.39	37.84±1.52	35.46±4.58	72.74	70.17±4.28	65.17±4.69
UEAI	63.89	58.71±3.10	55.29±7.68	**48.96**	38.04±3.35	**36.69**±8.29	84.79	79.32±2.05	75.28±2.56
AWGF	61.44	59.86±3.57	58.34±3.37	54.13	23.58±6.92	7.05±7.78	72.74	70.17±4.28	65.17±4.69
IMSR	58.72	44.71±9.17	42.81±4.12	27.55	35.46±6.80	34.81±5.95	83.12	80.54±4.71	77.57±4.27
PIMVC	**71.55**	61.33±4.27	60.66±3.32	28.16	28.11±4.91	27.10±2.46	**90.72**	**85.52**±1.10	78.61±2.52
SCSL	56.87	30.92±4.86	27.43±5.19	36.56	19.30±2.18	10.83±7.92	85.75	75.38±2.77	67.89±1.55
SFCR	69.54	**66.83**±3.35	**65.82**±2.85	47.14	**40.43**±2.04	35.25±2.45	89.49	84.64±2.64	**80.46**±2.40
Method \Ratio	ORL			Leaves			COIL100		
	0	20	30	0	20	30	0	20	30
BSV	88.62	72.97±0.68	66.87±0.98	81.18	68.38±0.26	61.66±0.38	83.49	70.45±0.19	64.58±0.11
UEAI	89.85	84.53±0.33	83.02±0.48	92.80	81.28±0.20	74.43±0.38	82.36	74.28±0.12	71.05±0.20
AWGF	80.74	76.65±0.64	72.82±1.32	88.90	80.72±0.67	78.37±0.73	83.06	80.48±1.03	79.15±0.34
IMSR	90.28	86.69±0.95	83.78±1.06	93.75	80.03±0.71	74.03±0.28	82.78	72.97±0.50	69.40±0.16
PIMVC	89.35	88.91±0.74	87.25±0.95	94.17	82.95±0.45	79.20±0.58	86.12	88.60±0.09	87.76±0.22
SCSL	90.21	86.81±1.41	84.28±0.97	-	-	-	-	-	-
SFCR	**95.26**	**90.95**±1.45	**88.08**±0.99	**95.38**	**87.14**±0.80	**80.35**±1.05	**93.70**	**91.25**±0.26	**89.99**±0.87

Table 3: Clustering performance of methods across varied missing ratios, where the best and second are in bold and underlined.

incapable handle Leaves and COIL100 (denoting by "-"). The following conclusions can be drawn: (1) As the missing ratio increases, the performance of all methods shows varying degrees of decrease, indicating that the truth relations among samples will be destroyed in the incomplete scenarios. In contrast, SFCR outperforms others and achieves more stable results across different missing ratios, fully demonstrating its effectiveness in incomplete multi-view clustering tasks. (2) Compared to the non-recovery methods (i.e., BSV, AWGF, PIMVC and SCSL), SFCR performs better in most cases, which highlights that the recovered samples with consistent structures indeed facilitate clustering. (3) SFCR achieves superior results over the recovery-based methods (i.e., UEAI and IMSR), proving that distinguishing samples from different views during the similarity fusion enhances the reliability of graph, thereby inducing a clear graph structure for clustering. Meanwhile, the computational complexity of all compared methods (except BSV) is presented in Table 5, and Table 6 records the running time. We find that SFCR can achieve competitive or better performance over state-of-the-art methods in computational efficiency.

Method \Ratio	ACC			NMI		
	0	20	30	0	20	30
BSV	5.50	6.00	6.00	5.33	5.83	5.67
UEAI	4.17	3.50	4.00	3.83	3.50	3.67
AWGF	4.67	4.50	4.17	4.50	4.83	4.67
IMSR	4.83	4.00	3.83	4.50	4.33	4.33
PIMVC	2.50	2.83	2.50	2.83	2.33	2.00
SCSL	5.17	5.83	6.17	5.17	5.83	5.83
SFCR	1.17	1.33	1.33	1.83	1.33	1.83

Table 4: Average ranks with different missing ratios, where SCSL ties for last place in Leaves and COIL100.

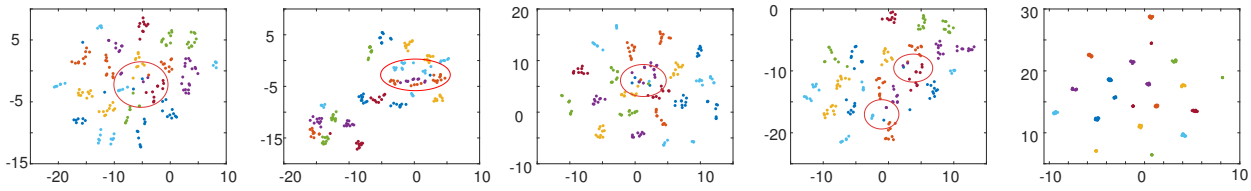

(a) UEAI (b) PIMVC (c) IMSR (d) SCSL (e) SFCR

Figure 3: T-SNE results of the unified representation on the ORL (no representation is learned from AWGF).

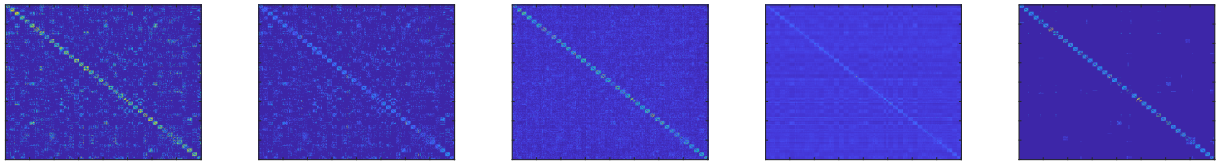

(a) Original S (b) AWGF (c) IMSR (d) SCSL (e) SFCR

Figure 4: The learned graphs of each method on the ORL, in which UEAI and PIMVC use a pre-constructed graph, i.e., (a).

Methods	Computational costs	Methods	Computational costs
UEAI	$\mathcal{O}(n^3+n^2d)$	AWGF	$\mathcal{O}(n^4+n^2d)$
IMSR	$\mathcal{O}(n^3+n^2d)$	PIMVC	$\mathcal{O}(n^3+nd^2)$
SCSL	$\mathcal{O}(n^3+n^2d)$	**SFCR**	$\mathcal{O}(n^3+n^2d)$

Table 5: Computational complexity of compared methods.

Datasets	UEAI	AWGF	IMSR	PIMVC	SCSL	**SFCR**
3sources	2.08	0.78	0.64	<u>0.14</u>	5.55	**0.12**
Webkb	0.25	0.48	0.28	<u>0.17</u>	0.61	**0.10**
MSRC-v1	0.15	0.81	0.33	<u>0.13</u>	1.03	**0.11**
ORL	<u>0.32</u>	1.63	1.16	0.34	4.38	**0.29**
Leaves	8.55	33.96	10.46	**5.33**	-	<u>5.87</u>
COIL100	37.11	151.82	38.52	**25.41**	-	<u>30.12</u>

Table 6: Running time (in seconds) of each method, where the best and second are in bold and underlined, respectively.

Visualization

To intuitively demonstrate the effectiveness of each method in exploring the information within incomplete multi-view data, the learned representations and graphs of different methods on the ORL with a fixed missing ratio of 20% are shown. Specifically, Figure. 3 displays the T-SNE visualization of the unified representation from 200 samples (Van der Maaten and Hinton 2008), while Figure. 4 shows the graph matrices. We observe that the visualizations of others (Figures. 3 (a)-(d)) display overlaps between different classes and cannot effectively separate them. Even worse, the learned graphs (Figures. 4 (a)-(d)) exhibit numerous connecting relations across multiple clusters, which negatively impacts the performance of clustering. In contrast, the unified representation of SFCR (Figure. 3 (e)) is more separable and the relations of different clusters are significantly reduced (Figure. 4 (e)), demonstrating that SFCR can learn the consistent similarity graph and use it to guide the representation learning, benefiting the ultimate clustering.

Ablation Study

To further verify the significance of collaborative similarity fusion and consistency recovery, an ablation study is conducted. Specifically, three variants of SFCR are designed: SFCR-1 removes the view-to-sample weights (i.e., α) and implicit weights (i.e., q^v) simultaneously; SFCR-2 only retains the similarity graph fusion model, excluding the consistency recovery; and SFCR-3, wherein the rank constraint is omitted, such that the learned graph lacks the property of exact connected components. Figure. 5 shows the ACC of SFCR as well as its distilled versions with the missing ratio fixed at 20% (more results are provided in Appendix), and we find that: (1) Compared with SFCR-1, SFCR consistently attains better performance, underscoring that measuring the importance of different views benefits the overall performance. (2) The results of SFCR outperform SFCR-2, which demonstrates that the discard of missing samples impairs the full utilization of data. (3) SFCR achieves a superior performance than SFCR-3, confirming that the clear similarity structure facilitates the ultimate clustering.

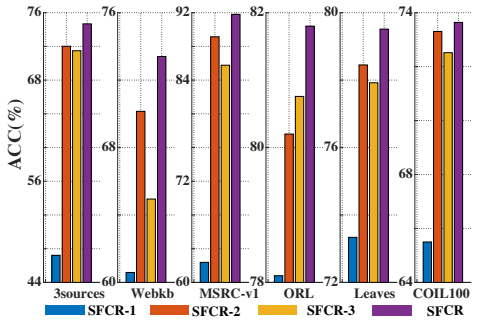

Figure 5: ACC of SFCR and its simplified versions.

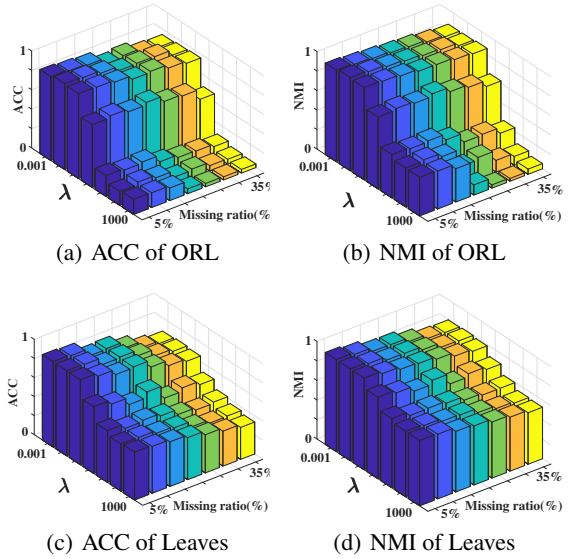

(a) ACC of ORL (b) NMI of ORL

(c) ACC of Leaves (d) NMI of Leaves

Figure 6: ACC with different λ and γ on Leaves and ORL.

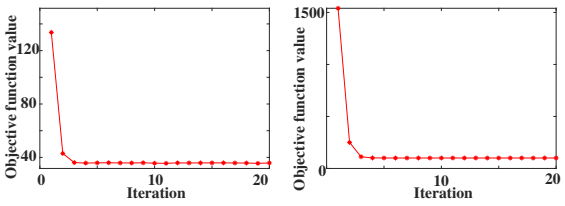

(a) ORL (b) Leaves

Figure 7: Variation curves of objective function values.

Parameter Sensitivity and Convergence

SFCR involves two intrinsic parameters, i.e., λ and β, where the parameter λ balances the consistent recovery and the similarity fusion, and β controls the impacts of rank constraint. Concretely, we dynamically update β during optimization procedures to satisfy the requirement of cluster number and tune λ manually. Therefore, to evaluate the effects of λ on SFCR, the ACC with different λ and varying missing ratios are presented in Figure. 6. Obviously, SFCR performs better, particularly when λ is smaller than 1, highlighting that distinguishing samples from different views indeed benefits the similarity graph learning. Meanwhile, to demonstrate the convergence of SFCR, Figure. 7 exhibits the objective function versus the number of iterations. From the results in Figure. 7, we can conclude that the objective function can converge to a stable value quickly.

Conclusion

In this paper, a novel collaborative Similarity Fusion and Consistent Recover (SFCR) method is designed to address the challenges of incomplete multi-view clustering. To fully utilize the potential information under the incomplete scenario, SFCR not only fuses the similarity graph through view-to-sample weights to distinguish the importance of different samples but also employs the consistent graph to recover missing samples, thereby effectively enhancing the quality of the learned graph and maintaining the locality of recovered samples. Further, the final clustering labels can be obtained directly without requiring additional clustering processes. Extensive experiments underscore the superiority of SFCR when handling incomplete multi-view clustering. In the future, we will extend SFCR to identify representative features, achieving multi-view feature selection in the incomplete scenarios. Moreover, designing an efficient framework to extend the scalability of SFCR is crucial for real-world applications.

Acknowledgments

This work was supported in part by the National Key R&D Plan of China under Grant No.2024YFE0202700, in part by the National Natural Science Foundation of China under Grants U2433216, 62306171, 62176001 and 62306282, in part by the Science and Technology Major Project of Shanxi Province under Grant 202201020101006, in part by the Natural Science Foundation of Jiangsu Province under Grant BK20231337, and in part by the the Modern Agricultural Machinery Equipment and Technology Extension Project of Jiangsu Province under Grant NJ2024-06.

References

Cao, Z.; and Xie, X. 2024. Partition-Level Tensor Learning-Based Multiview Unsupervised Feature Selection. *IEEE Transactions on Neural Networks and Learning Systems*.

Deng, S.; Wen, J.; Liu, C.; Yan, K.; Xu, G.; and Xu, Y. 2024. Projective incomplete multi-view clustering. *IEEE Transactions on Neural Networks and Learning Systems*, 35(08): 10539–10551.

Fan, K. 1949. On a theorem of Weyl concerning eigenvalues of linear transformations I. In *Proceedings of the National Academy of Sciences*, 652–655.

Fu, P.; Liang, X.; Qian, Y.; Guo, Q.; Zhang, Y.; Huang, Q.; and Tang, K. 2024. Multi-Scale Features Are Effective for Multi-Modal Classification: An Architecture Search Viewpoint. *IEEE Transactions on Circuits and Systems for Video Technology*.

Gan, J.; Hu, R.; Zhan, M.; Mo, Y.; Wan, Y.; and Zhu, X. 2022. Multi-view Unsupervised Graph Representation Learning. In *Proceedings of the International Joint Conference on Artificial Intelligence*, 2987–2993.

Hestenes, M. R. 1969. Multiplier and gradient methods. *Journal of Optimization Theory and Applications*, 4(5): 303–320.

Hu, R.; Peng, L.; Gan, J.; Shi, X.; and Zhu, X. 2022. Complementary graph representation learning for functional neuroimaging identification. In *Proceedings of the ACM International Conference on Multimedia*, 3385–3393.

Jiang, B.; Wu, X.; Zhou, X.; Cohn, A. G.; Liu, Y.; Sheng, W.; and Chen, H. 2024. Semi-Supervised Multi-View Feature Selection with Adaptive Graph Learning. *IEEE Trans-*

actions on Neural Networks and Learning Systems, 35(3): 3615–3629.

Jiang, B.; Xiang, J.; Wu, X.; He, W.; Hong, L.; and Sheng, W. 2021. Robust adaptive-weighting multi-view classification. In *Proceedings of the ACM International Conference on Information & Knowledge Management*, 3117–3121.

Jiang, B.; Zhang, C.; Zhong, Y.; Liu, Y.; Zhang, Y.; Wu, X.; and Sheng, W. 2023. Adaptive collaborative fusion for multi-view semi-supervised classification. *Information Fusion*, 96: 37–50.

Jiang, Z.; Luo, T.; and Liang, X. 2024. Deep Incomplete Multi-View Learning Network with Insufficient Label Information. In *Proceedings of the AAAI Conference on Artificial Intelligence*, 12919–12927.

Li, S.; Jiang, Y.; and Zhou, Z. 2014. Partial multi-view clustering. In *Proceedings of the AAAI Conference on Artificial Intelligence*, 1968–1974.

Li, X.; Zhang, H.; Wang, R.; and Nie, F. 2022. Multiview clustering: A scalable and parameter-free bipartite graph fusion method. *IEEE Transactions on Pattern Analysis and Machine Intelligence*, 44(1): 330–344.

Liang, X.; Fu, P.; Guo, Q.; Zheng, K.; and Qian, Y. 2024. DC-NAS: Divide-and-Conquer Neural Architecture Search for Multi-Modal Classification. In *Proceedings of the AAAI Conference on Artificial Intelligence*, 13754–13762.

Liu, J.; Liu, X.; Zhang, Y.; Zhang, P.; Tu, W.; Wang, S.; Zhou, S.; Liang, W.; Wang, S.; and Yang, Y. 2021. Self-representation subspace clustering for incomplete multi-view data. In *Proceedings of the ACM International Conference on Multimedia*, 2726–2734.

Liu, S.; Zhang, J.; Wen, Y.; Yang, X.; Wang, S.; Zhang, Y.; Zhu, E.; Tang, C.; Zhao, L.; and Liu, X. 2024. Sample-Level Cross-View Similarity Learning for Incomplete Multi-View Clustering. In *Proceedings of the AAAI Conference on Artificial Intelligence*, 14017–14025.

Mohar, B.; Alavi, Y.; Chartrand, G.; and Oellermann, O. 1991. The Laplacian spectrum of graphs. *Graph theory, combinatorics, and applications*, 2(871-898): 12.

Nie, F.; Wang, X.; and Huang, H. 2014. Clustering and projected clustering with adaptive neighbors. In *Proceedings of the ACM SIGKDD International Conference on Knowledge Discovery and Data Mining*, 977–986.

Trivedi, A.; Rai, P.; Daumé III, H.; and DuVall, S. L. 2010. Multiview clustering with incomplete views. In *workshop of the Neural Information Processing Systems*, 1–8.

Van der Maaten, L.; and Hinton, G. 2008. Visualizing data using t-SNE. *Journal of Machine Learning Research*, 9(11): 2579–2605.

Wang, H.; Yang, Y.; and Liu, B. 2020. GMC: Graph-based multi-view clustering. *IEEE Transactions on Knowledge and Data Engineering*, 32(6): 1116–1129.

Wang, J.; Feng, S.; Lyu, G.; and Yuan, J. 2024a. SURER: Structure-Adaptive Unified Graph Neural Network for Multi-View Clustering. In *Proceedings of the AAAI Conference on Artificial Intelligence*, 15520–15527.

Wang, Z.; Li, L.; Ning, X.; Tan, W.; Liu, Y.; and Song, H. 2024b. Incomplete multi-view clustering via structure exploration and missing-view inference. *Information Fusion*, 103: 102123.

Wen, J.; Deng, S.; Fei, L.; Zhang, Z.; Zhang, B.; Zhang, Z.; and Xu, Y. 2022. Discriminative regression with adaptive graph diffusion. *IEEE Transactions on Neural Networks and Learning Systems*, 35(2): 1797–1809.

Wen, J.; Zhang, Z.; Xu, Y.; Zhang, B.; Fei, L.; and Liu, H. 2019. Unified embedding alignment with missing views inferring for incomplete multi-view clustering. In *Proceedings of the AAAI Conference on Artificial Intelligence*, 5393–5400.

Xue, Z.; Du, J.; Zheng, C.; Song, J.; Ren, W.; and Liang, M. 2021. Clustering-Induced Adaptive Structure Enhancing Network for Incomplete Multi-View Data. In *Proceedings of the International Joint Conference on Artificial Intelligence*, 3235–3241.

Xue, Z.; Li, G.; Wang, S.; Huang, J.; Zhang, W.; and Huang, Q. 2019. Beyond global fusion: A group-aware fusion approach for multi-view image clustering. *Information Sciences*, 493: 176–191.

Yin, J.; and Sun, S. 2023. Incomplete multi-view clustering with reconstructed views. *IEEE Transactions on Knowledge and Data Engineering*, 35(3): 2671–2682.

Zhan, K.; Zhang, C.; Guan, J.; and Wang, J. 2018. Graph learning for multiview clustering. *IEEE Transactions on Cybernetics*, 48(10): 2887–2895.

Zhang, C.; Fang, Y.; Liang, X.; Zhang, H.; Zhou, P.; Wu, J., Xingyu andYang; Jiang, B.; and Sheng, W. 2024a. Efficient Multi-view Unsupervised Feature Selection with Adaptive Structure Learning and Inference. In *Proceedings of the International Joint Conference on Artificial Intelligence*, 5443–5452.

Zhang, C.; Jiang, B.; Wang, Z.; Yang, J.; Lu, Y.; Wu, X.; and Sheng, W. 2023a. Efficient multi-view semi-supervised feature selection. *Information Sciences*, 649: 119675.

Zhang, C.; Li, H.; Lv, W.; Huang, Z.; Gao, Y.; and Chen, C. 2023b. Enhanced tensor low-rank and sparse representation recovery for incomplete multi-view clustering. In *Proceedings of the AAAI Conference on Artificial Intelligence*, 11174–11182.

Zhang, C.; Zhu, X.; Wang, Z.; Zhong, Y.; Sheng, W.; Ding, W.; and Jiang, B. 2024b. Discriminative Multi-View Fusion via Adaptive Regression. *IEEE Transactions on Emerging Topics in Computational Intelligence*, 8(6): 3821–3833.

Zhang, P.; Wang, S.; Hu, J.; Cheng, Z.; Guo, X.; Zhu, E.; and Cai, Z. 2020. Adaptive weighted graph fusion incomplete multi-view subspace clustering. *Sensors*, 20(20): 5755.